Journal of Magnetic Resonance 308 (2019) 106595

Contents lists available at ScienceDirect

Journal of Magnetic Resonance

journal homepage: www.elsevier.com/locate/jmr

Spin Lock Adiabatic Correction (SLAC) for B_1-insensitive pulse design at 7T

Edward M. Green [a,b,*], Yasmin Blunck [a,b], Bahman Tahayori [b,c,d], Peter M. Farrell [e], James C. Korte [b,f,1], Leigh A. Johnston [a,b,1]

[a] Melbourne Brain Centre Imaging Unit, The University of Melbourne, Melbourne, VIC, Australia
[b] Department of Biomedical Engineering, The University of Melbourne, Melbourne, VIC, Australia
[c] Department of Medical Physics and Biomedical Engineering, Shiraz University of Medical Sciences, Shiraz, Iran
[d] Center for Neuromodulation and Pain, Shiraz, Iran
[e] Department of Electrical and Electronic Engineering, The University of Melbourne, Melbourne, VIC, Australia
[f] Department of Physical Sciences, Peter MacCallum Cancer Centre, Melbourne, VIC, Australia

ARTICLE INFO

Article history:
Received 30 April 2019
Revised 9 August 2019
Accepted 8 September 2019
Available online 11 September 2019

Keywords:
RF excitation
B_1 inhomogeneity
Adiabatic pulse
MRI
Frequency-modulated

ABSTRACT

A new framework for B_1 insensitive adiabatic pulse design is proposed, denoted Spin Lock Adiabatic Correction (SLAC), which counteracts deviations from ideal behaviour through inclusion of an additional correction component during pulse design. SLAC pulses are theoretically derived, then applied to the design of enhanced BIR-4 and hyperbolic secant pulses to demonstrate practical utility of the new pulses. At 7T, SLAC pulses are shown to improve the flip angle homogeneity compared to a standard adiabatic pulse with validation in both simulations and phantom experiments, under SAR equivalent experimental conditions. The SLAC framework can be applied to any arbitrary adiabatic pulse to deliver excitation with increased B_1 insensitivity.

1. Introduction

The use of greater static magnetic field strength in magnetic resonance imaging (MRI) facilitates acquisition of images with higher signal-to-noise ratio (SNR). At 7T and beyond, however, this improvement is undermined by the excitation wavelength causing interference and dielectric resonances that result in an inhomogeneous B_1 field throughout the object being imaged [1,2]. The heterogeneous excitation field causes inconsistency in image contrast as flip angles vary across the object. Efforts have been made to overcome B_1 inhomogeneity using post-processing [3,4], multiple channel transmit array coils [5,6] and pulse design [7–9].

Frequency swept pulses have been used for decades to overcome inhomogeneous B_1 fields. Much of this work has been in the form of adiabatic pulses, in which the magnetisation follows a sweeping effective field when the RF amplitude exceeds a given threshold at which the adiabatic condition is satisfied [10]. Developments over the years have increased the utility of adiabatic pulses such that they can be used for excitation with arbitrary flip angles [11], slice-selective inversion [12], refocusing pulses [13] and slice-selective excitation [14–16]. Further progress in frequency-modulated (FM) pulses has led to pulses which depend on the weighting given to their trajectory through excitation k-space to achieve B_1 insensitivity [17–20]. With these developments, adiabatic pulses have extended the utility of a range of imaging sequences to be applicable to conditions with significant RF transmit inhomogeneity.

The performance of adiabatic pulses can be defined as how well magnetisation follows the trajectory of the effective field produced by the pulse. This may be improved by increasing pulse amplitude or increasing pulse duration, however this comes at the expense of greater specific absorption rate (SAR). Also crucial for optimising the performance of an adiabatic pulse is choice of amplitude and phase modulation functions. Examples of such functions are sech/tanh [12], tanh/tan [21] and sin/cos [22]. Modifications to these well known analytical functions can produce improvements in both B_1 and B_0 insensitivity [23,24].

* Corresponding author at: Melbourne Brain Centre Imaging Unit, Kenneth Myer Building, University of Melbourne, 30 Royal Parade, Parkville, VIC 3052, Australia.
E-mail addresses: egreen@student.unimelb.edu.au (E.M. Green), bluncky@unimelb.edu.au (Y. Blunck), tahayori@sums.ac.ir (B. Tahayori), pfarrell@unimelb.edu.au (P.M. Farrell), james.korte@petermac.org (J.C. Korte), l.johnston@unimelb.edu.au (L.A. Johnston).
[1] These authors have contributed equally.

https://doi.org/10.1016/j.jmr.2019.106595
1090-7807/

A new avenue for extending the B_1 insensitivity of adiabatic pulses is proposed, involving the introduction of an additional component to dynamically reduce the deviation from the desired trajectory by creating a spin lock in an excitation frame of reference. This approach of Spin Lock Adiabatic Correction (SLAC) thus defines a new class of pulses that by design lead to increased flip angle homogeneity in high field environments. We present a derivation of the SLAC principle and analyse its characteristics using the superadiabiticity framework [25]. We demonstrate SLAC performance in both simulation and experiment at 7T, building on the exemplars of a BIR-4 adiabatic pulse [11] and a hyperbolic secant (HS) pulse [12].

2. Theory

Consider an arbitrary adiabatic pulse defined by amplitude $B_1^{\mathrm{e,Ad}}(t)$, phase $\phi^{\mathrm{Ad}}(t)$, and duration T_{p},

$$B_1^{\mathrm{Ad}}(t) = B_1^{\mathrm{e,Ad}}(t)e^{i\phi^{\mathrm{Ad}}(t)}, \quad 0 \leqslant t \leqslant T_{\mathrm{p}}. \tag{1}$$

Adiabatic pulses are known to be tolerant of both B_0 and B_1 inhomogeneity. An important factor in pulse design at high field is to maximise tolerance to B_1 inhomogeneity. In the following, we will denote by ξ the B_1 field weighting factor that relates the B_1 strength at a reference point in space to the B_1 strength at an arbitrary location in space.

In the frequency-modulated frame (Fig. 1a) with x'-axis locked to $\phi^{\mathrm{Ad}}(t)$, the effective field produced by an adiabatic pulse, $B_{\mathrm{eff}}^{\mathrm{Ad}}$, makes an angle α with the B_0 field, where

$$\alpha(\xi, t) = \arctan\left(\frac{\gamma\,\xi\, B_1^{\mathrm{e,Ad}}(t)}{\Delta\omega(t)}\right), \tag{2}$$

and

$$\Delta\omega(t) = \frac{d\phi^{\mathrm{Ad}}}{dt}, \tag{3}$$

where γ is the gyromagnetic ratio. Note the explicit dependence of angle α on the B_1 field weighting factor, ξ; this is a crucial factor moving forward.

The adiabatic condition is achieved when the effective field is swept sufficiently slowly that the magnetisation follows the effective field. In practice, however, B_1 inhomogeneity and finite pulse duration cause the magnetisation to deviate from the effective field. The deviation that occurs over the course of the adiabatic pulse is dependent on the rate at which $B_{\mathrm{eff}}^{\mathrm{Ad}}$ is swept, $\frac{d\alpha}{dt}$. Our proposed method of Spin Lock Adiabatic Correction applies an additional field, of amplitude $B_1^{\mathrm{e,SL}}$, to reduce the deviation:

$$B_1^{\mathrm{SLAC}}(t) = \left(B_1^{\mathrm{e,Ad}}(t) + iB_1^{\mathrm{e,SL}}(t)\right)e^{i\phi^{\mathrm{Ad}}(t)} \tag{4}$$

The correcting component is chosen with reference to a nominal B_1 field factor, $\xi = \xi^{\mathrm{ref}}$:

$$B_1^{\mathrm{e,SL}}(t) = -\frac{1}{\gamma\xi^{\mathrm{ref}}}\frac{d\alpha\left(\xi^{\mathrm{ref}}, t\right)}{dt} \tag{5}$$

The first adiabatic frame aligns $B_{\mathrm{eff}}^{\mathrm{Ad}}$ with the z''-axis, and is indicated by double prime notation (Fig. 1b). Let E be the effective field in this frame. The goal of SLAC is to minimise ϵ, the angle between $B_{\mathrm{eff}}^{\mathrm{Ad}}$ and E, as demonstrated in Fig. 1c. The result of applying the additional SL component is to achieve greater fidelity in the magnetisation trajectories. The cone angle ϵ is defined by

$$\epsilon(t) = \arctan\left(\frac{||\frac{d\alpha}{dt}\,\mathbf{e}_{y'} + \gamma\mathbf{B}_1^{\mathrm{SL}}(t)||_2}{||\gamma\mathbf{B}_{\mathrm{eff}}^{\mathrm{Ad}}(t)||_2}\right) \tag{6}$$

where $\mathbf{e}_{y'}$ is a unit vector in the y'-direction.

For a chosen nominal field weighting factor, $\xi = \xi^{\mathrm{ref}}$, the SLAC pulse perfectly cancels the trajectory deviation, resulting in an optimal cone angle, $\epsilon = 0$.

In general, the addition of $\mathbf{B}_1^{\mathrm{SL}}$ leads to greater B_1 amplitudes in SLAC-optimised pulses, consequently resulting in a higher energy deposition. In order to maintain equal SAR exposure, the SLAC pulse amplitude is linearly rescaled to match the power of the underlying adiabatic base-pulse:

$$\overline{\mathbf{B}}_1^{\mathrm{SLAC}}(t) = \mathbf{B}_1^{\mathrm{SLAC}}(t)\sqrt{\frac{\int_0^{T_{\mathrm{p}}}||\mathbf{B}_1^{\mathrm{Ad}}(t)||_2^2 dt}{\int_0^{T_{\mathrm{p}}}||\mathbf{B}_1^{\mathrm{Ad}}(t)||_2^2 + ||\mathbf{B}_1^{\mathrm{SL}}(t)||_2^2 dt}} \tag{7}$$

where $\overline{\mathbf{B}}_1^{\mathrm{SLAC}}$ is the rescaled field.

3. Methods

SLAC was applied to two widely used adiabatic pulses, the BIR-4 pulse, which enables plane rotations of arbitrary flip angle by locking magnetisation in a plane orthogonal to the effective field [11], and the hyperbolic secant pulse [12], a widely used adiabatic full passage (AFP) pulses, in order to assess its effect on pulse performance in simulations and experiments. Excitation performance was assessed using BIR-4, SLAC-BIR-4 and SAR-matched SLAC-BIR-4 pulses. Inversion performance was assessed using HS, SLAC-HS and SAR-matched SLAC-HS pulses. Standard block pulses of duration T_{p} = 0.5 ms and 1 ms were used as references for excitation and inversion respectively.

The nominal flip angle of the BIR-4 pulse was set to $\theta = 45°$ and the four BIR-4 pulse segments were derived from tanh/tan adiabatic half passages (AHP) with parameters ζ = 20, κ = arctan(20), $\Delta\omega_{\max}/2\pi$ = 5 kHz applied to equations defined by [21] (see Appendix). These parameter choices were made in order to

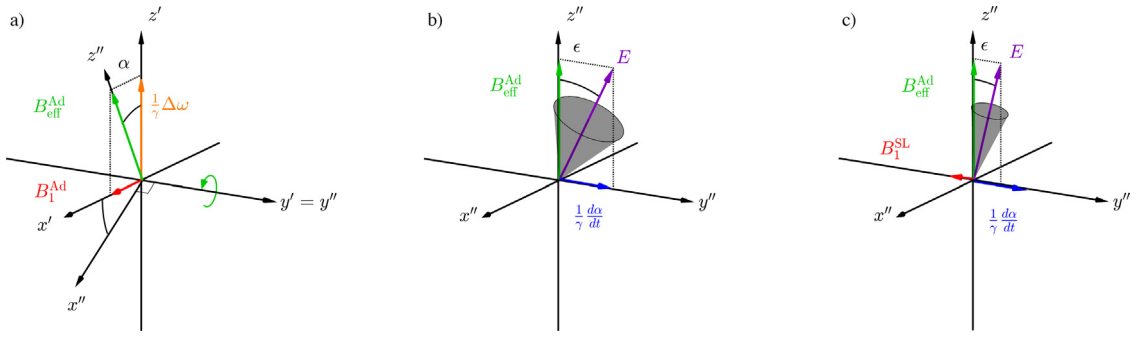

Fig. 1. Rotating frames of reference. (a) The frequency modulated (FM) frame: the effective field is swept as off-resonance frequency of excitation, $\Delta\omega$, and amplitude, B_1^{Ad}, vary. (b) The $B_{\mathrm{eff}}^{\mathrm{Ad}}$ frame: the angle between effective field in this frame and $B_{\mathrm{eff}}^{\mathrm{Ad}}$ is dependent on the sweep rate in the FM frame during an adiabatic pulse. (c) The $B_{\mathrm{eff}}^{\mathrm{Ad}}$ frame: The cone angle, ϵ, is decreased when B_1^{SL} is applied.

approximate a set of equations derived using the numerically optimised modulation (NOM) procedure [23]. Each segment was individually SLAC-optimised to produce the SLAC-BIR-4 pulse. The nominal B_1 field weighting factor, ξ^{ref}, used for the SLAC-optimisation was selected based on the simulation. It was set where the BIR-4 pulse simulated with the same pulse duration and reference B_1 strength produced 95% of the transverse magnetisation corresponding to the desired flip angle. Choosing a percentage of transverse magnetisation much lower than 95% requires too large a correction component with increased B_1 sensitivity (Fig. 3a). 95% of transverse magnetisation roughly corresponds to a field weighting factor threshold, ξ, at which correction using B_1^{SL} produces good results (Fig. 3b). Choosing a value closer to 100% results in a trivially small correction component being employed (Fig. 3c).

The HS pulse used was a vendor-provided HS pulse (Siemens Healthineers, Erlangen, Germany) with parameters μ = 975.5 and β = 3.4516 corresponding to $\Delta\omega_{max}/2\pi$ = 535 Hz with a pulse duration T_p = 10.24 ms applied to equations as found in [8] (see Appendix). The nominal B_1 field weighting factor, ξ^{ref} = 0.7, used for the SLAC-optimisation was selected based on the simulation.

3.1. Simulation

Simulations of block, BIR-4, SLAC-BIR-4, HS and SLAC-HS pulses were performed in MATLAB (Natick, Massachusetts, USA) via numerical integration of the Bloch equations with relaxation parameters of T_1 = 1 s and T_2 = 0.5 s. BIR-4 and SLAC-BIR-4 pulse shapes were calculated over a range of pulse durations (4–11 ms) and pulse amplitudes with reference B_1 strength, $\omega_1^{ref}/2\pi$ = (100–300 Hz), corresponding to the maximum amplitude of a BIR-4 pulse. HS and SLAC-HS pulse shapes were calculated for $\omega_1^{ref}/2\pi$ = 500 Hz corresponding to the maximum amplitude of a HS pulse. Both unscaled pulses and SAR-matched pulses were simulated for both SLAC-BIR-4 and SLAC-HS. Computations were conducted over the range of B_1 field weighting factor, $\xi \in [0.5, 1.5]$. The metric used to assess the performance of the excitation pulses was the mean over the simulated B_1 strength range of the magnitude of transverse magnetisation produced by the pulse normalised by the desired transverse magnetisation,

$$C_{xy} = \int_{0.5}^{1.5} \frac{||M_{xy}(\mathbf{B}_1(T_p), \xi)||_2}{\sin(\theta)} d\xi \tag{8}$$

where $\mathbf{B}_1(T_p)$ is the particular pulse being evaluated at T_p.

The metric used to assess the performance of the inversion pulses was the mean over the simulated B_1 strength range of the longitudinal magnetisation produced by the pulse,

$$C_z = \int_{0.5}^{1.5} M_z(\mathbf{B}_1(T_p), \xi) d\xi \tag{9}$$

Further simulation was performed to demonstrate the effect of SLAC on off-resonance performance of pulses. The effects of pulses were simulated across an off-resonance range $\Delta\omega_0/2\pi$ = (−10 kHz

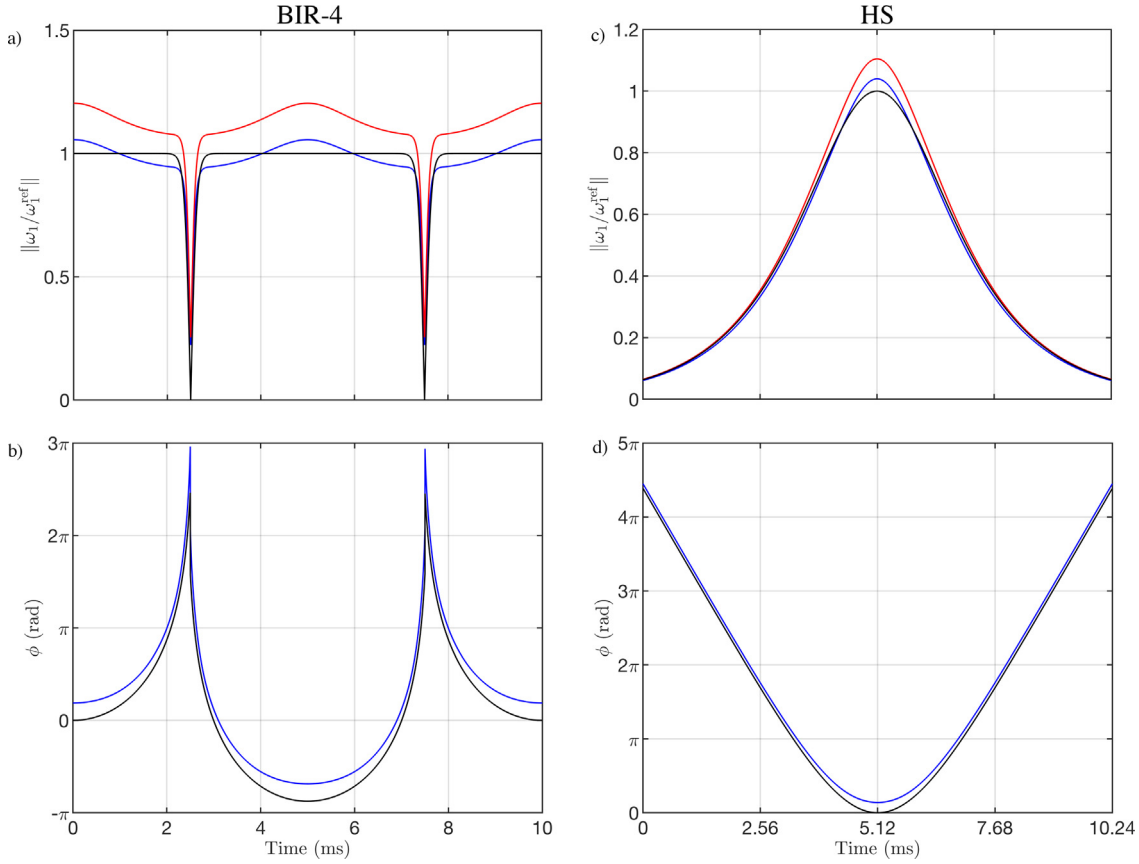

Fig. 2. (a) B_1 amplitude over the duration of the pulse for BIR-4 (black), unscaled SLAC-BIR-4 (red) and scaled SLAC-BIR-4 (blue), normalised by maximum amplitude of the BIR-4 pulse. (b) Phase of B_1 over the duration of the pulse for BIR-4 (black) and SLAC-BIR-4 (blue). The phase difference between SLAC-BIR-4 and BIR-4 envelopes varies between 0 and $\pi/2$ as the proportions of orthogonal field components, B_1^{SL} and B_1^{Ad}, vary throughout the pulse with the maximum phase difference occurring at $T_p/4 = 2.5$ ms and $3T_p/4 = 7.5$ ms. (c) B_1 amplitude over the duration of the pulse for HS (black), unscaled SLAC-HS (red) and scaled SLAC-HS (blue), normalised by maximum amplitude of the HS pulse. (d) Phase of B_1 over the duration of the pulse for HS (black) and SLAC-HS (blue). (For interpretation of the references to colour in this figure legend, the reader is referred to the web version of this article.)

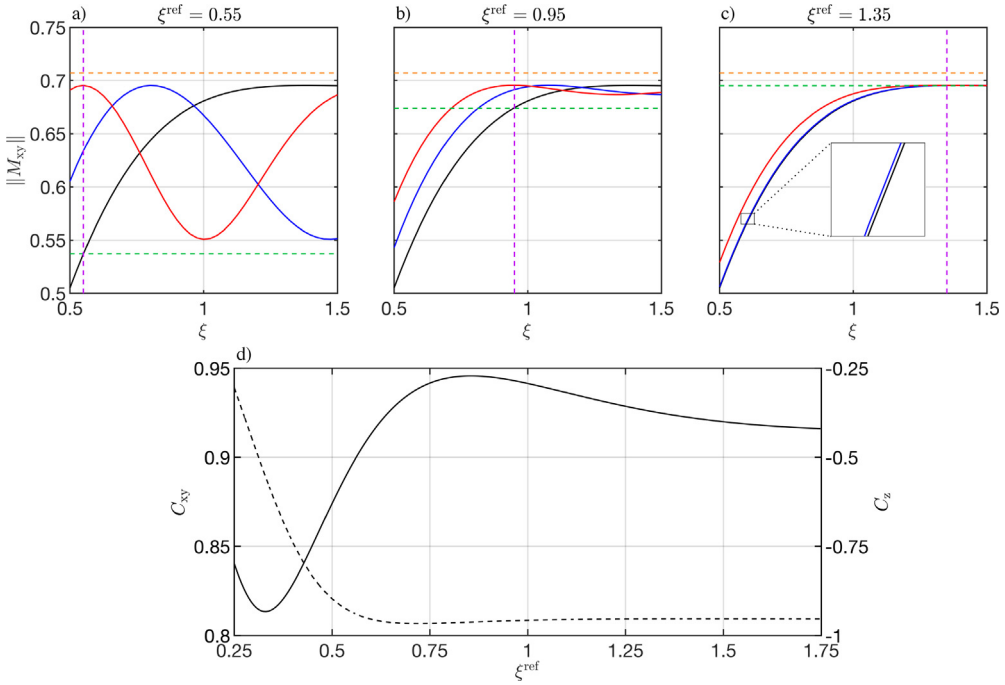

Fig. 3. Performance dependence on choice of B_1 field amplitude factor, ξ^{ref}, used for tuning B_1^{SL} for unscaled SLAC-BIR-4 (red) and SAR-matched SLAC-BIR-4 (blue) compared to BIR-4 (black). Example choices: (a) ξ^{ref} = 0.55 (b) ξ^{ref} = 0.95 (c) ξ^{ref} = 1.35. Flip angle $\theta = 45°$. Dashed orange line: Target $M_{xy} = \sin(45°)$. Dashed purple line: ξ^{ref}. Dashed green line: M_{xy} produced by BIR-4 pulse at ξ^{ref}. (d) Dependence of C_{xy} on ξ^{ref} for a SAR-matched SLAC-BIR-4 pulse (solid line) and dependence of C_z on ξ^{ref} for a SAR-matched HS pulse (dashed line). (For interpretation of the references to colour in this figure legend, the reader is referred to the web version of this article.)

to 10 kHz) and RF amplitude corresponding to $\xi\omega_1^{ref}/2\pi$ = (0–10 kHz), with the maximum amplitude of an adiabatic pulse, $\omega_1^{ref}/2\pi$ = 200 Hz in the case of the simulated BIR-4 pulse and $\omega_1^{ref}/2\pi$ = 500 Hz in the case of the simulated HS pulse.

Additionally, the performance was analysed in superadiabatic frames for BIR-4, SLAC-BIR-4, HS and SLAC-HS at $\xi = 1$. This analysis concerns the cone angle defined by the effective field in an adiabatic frame of reference, e.g. ϵ in Fig. 1b/c, and helps to assess the potential flip angle inaccuracy of any adiabatic pulse. The $(n+1)$th adiabatic frame is defined as being locked to the effective field in the nth frame. For frames of reference beyond the first adiabatic frame the convention of [25] is followed and the cone angle in the nth frame is denoted by α_n.

3.2. Experiments

Data were acquired on a research 7T MRI (Siemens Healthineers, Erlangen, Germany) using a single-channel TX-RX volume coil (QED, Mayfield Village, Ohio, USA). Experiments were performed on a Siemens spherical spectroscopy phantom (8.2 g Na $C_2H_3O_2$ + 9.6 g $C_3H_5O_3$ Li per 1000 g H_2O).

Volume images were obtained using a 0.5 ms block pulse, and BIR-4 and SAR-matched SLAC-BIR-4 pulses with T_p = 10 ms, ω_1^{ref} = 200 Hz, $\xi^{ref} = 0.95$. The resulting amplitude and phase functions are visualised in Fig. 2(a–b). Each pulse experiment was acquired with a custom-built 3D GRE-readout with parameters: TR = 5000 ms, TE = 10 ms, BW = 260 Hz, FOV = 200 mm isotropic, matrix size 256 × 128 × 64, total scan time = 11h23m.

Single slice images were obtained by applying an inversion pulse followed by spoiling of residual transverse magnetisation, then a sinc pulse excitation and readout. A 1 ms block pulse, and HS and SAR-matched SLAC-HS pulses with T_p = 10.24 ms, $\omega_1^{ref}/2\pi$ = 500 Hz, $\xi^{ref} = 0.7$, were used as inversion pulses. The resulting amplitude and phase functions are visualised in Fig. 2(c–d). Each pulse experiment was acquired with a 2D GRE-readout with parameters: TR = 5000 ms, TE = 10 ms, slice thickness = 3 mm, BW = 260 Hz, FOV = 200 mm isotropic, matrix size 256 × 128, total scan time = 20.2 m.

B_1 maps were estimated from two single-slice GRE images at 45° and 90° using a double-angle method [26]. TR = 10000 ms, TE = 10 ms, slice thickness = 3 mm, FOV = 200 × 200mm, matrix size = 256 × 128.

4. Results

SLAC optimisation targets a reduction of the cone angle, ϵ (Fig. 1c). Superadiabatic analysis was performed to investigate this aperture in the first three adiabatic frames for BIR-4 and SLAC-BIR-4 (Fig. 4) and for HS and SLAC-HS at ξ = 1. The unscaled and SAR-matched SLAC-BIR-4 result in smaller cone angles in the first two frames compared with standard BIR-4 pulse. The unscaled SLAC-BIR-4 pulse also produces a smaller maximal cone angle in the third adiabatic frame than a standard BIR-4 pulse. The frame with the lowest maximum angle for SLAC-BIR-4 suggests a small flip angle error of the SLAC-corrected pulse shape at ξ = 1 due to the cone angles being smaller than those of the standard BIR-4. The unscaled and SAR-matched SLAC-HS pulses result in smaller cone angles for the majority of the pulse duration in all three frames compared with the standard HS pulse, however, they have greater maximal cone angle in all of these scenarios aside from the SAR-matched SLAC-HS in the first frame. The smaller maximal cone angles of the HS pulse compared to the SLAC-HS pulse in the second and third order frames suggests a smaller flip angle error from the original HS pulse shape at ξ = 1. These assessments based on superadiabatic behaviour agree with the performance in simulation of the pulses. Flip angle error of unscaled and SAR-matched SLAC-BIR-4 pulses was smaller than that of BIR-4 pulses at ξ = 1, while the flip angle error of HS was smaller than that of unscaled and SAR-matched SLAC-HS at ξ = 1 (Fig. 5).

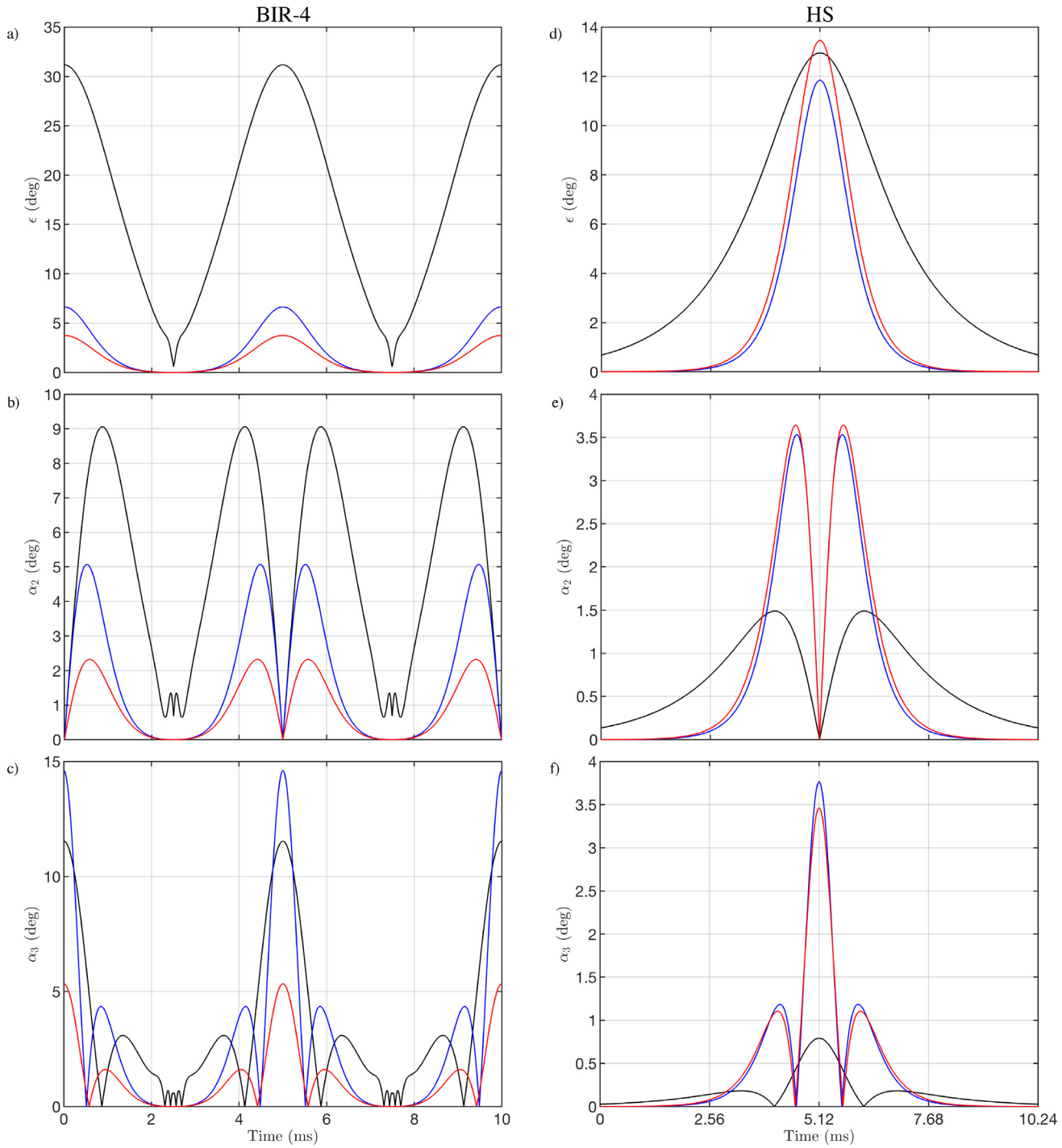

Fig. 4. (a–c) Superadiabatic behaviour of BIR-4 (black), SLAC-BIR-4 (red) and SAR-matched SLAC-BIR-4 (blue) for $\xi = 1$. Cone angle in the (a) first, (b) second and (c) third adiabatic frames. (d–f) Superadiabatic behaviour of HS (black), SLAC-HS (red) and SAR-matched SLAC-HS (blue) for $\xi = 1$. Cone angle in the (d) first, (e) second and (f) third adiabatic frames. (For interpretation of the references to colour in this figure legend, the reader is referred to the web version of this article.)

Simulations were used to investigate the effect of field weighting factor to which B_1^{SL} is tuned, ξ^{ref}, on the pulse performance across the B_1 field strength range with a target flip angle of $\theta = 45^\circ$ for BIR-4 and $\theta = 180^\circ$ for HS (Fig. 3). The simulation results reveal large variance in transverse magnetisation across the simulated field weighting factor range if ξ^{ref} is chosen to be small. $\xi^{ref} = 0.55$ corresponds to BIR-4 producing 76% of target M_{xy}, therefore the contribution from B_1^{SL} is large (Fig. 3a). For a chosen ξ^{ref}, SLAC-optimisation achieves flip angles closer to the target magnetisation across the ξ range. $\xi^{ref} = 0.95$ corresponds to BIR-4 producing 95% of target M_{xy}, therefore the contribution from B_1^{SL} is moderate (Fig. 3b). If ξ^{ref} is chosen to be high changes to performance are slight. $\xi^{ref} = 1.35$ corresponds to BIR-4 producing 98% of target M_{xy}, therefore the contribution from B_1^{SL} is small (Fig. 3c). For comparison, the block pulse reaches the target magnetisation at the reference field weighting, $\xi = 1$, with strong under and overshoot for ξ diverting from this reference (Fig. 5). While the mean magnitude of transverse magnetisation C_{xy}, varies nonlin-

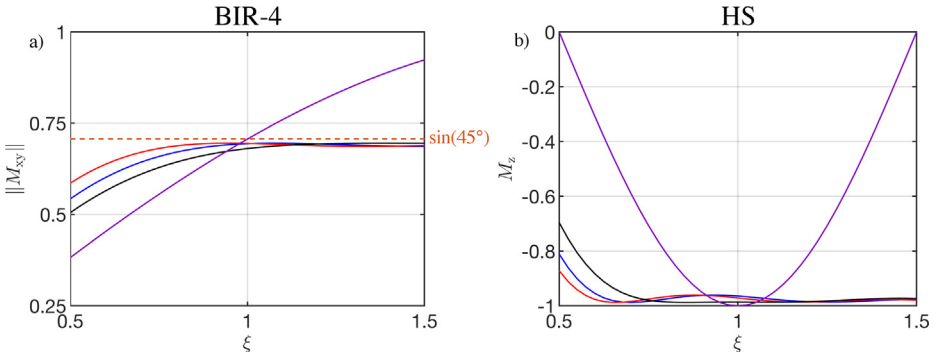

Fig. 5. (a) Transverse magnetisation vs. field weighting factor ξ following a 45° BIR-4 pulse (black), SAR-matched SLAC-BIR-4 pulse (blue), SLAC-BIR-4 pulse (red) and block pulse (purple). T_p = 10 ms, ω_1^{ref} = 200 Hz, $\xi^{ref} = 0.95$. The BIR-4, SLAC-BIR-4 and SAR-matched SLAC-BIR-4 produce transverse magnetisation close to that obtained from a perfect 45° flip for $\xi \geqslant 1$. As ξ decreases below 1 the transverse magnetisation decreases for these frequency swept pulses, with the decrease largest for the BIR-4 and the second largest decrease for the SAR-matched SLAC-BIR-4. The block pulse underflips for low ξ, flips accurately to 45° for $\xi = 1$ and overflips for high ξ. (b) Longitudinal magnetisation vs. field weighting factor ξ following a HS pulse (black), SAR-matched SLAC-HS pulse (blue), SLAC-HS pulse (red) and block pulse (purple). T_p = 10 ms, ω_1^{ref} = 200 Hz, $\xi^{ref} = 0.95$. The HS, SLAC-HS and SAR-matched SLAC-HS produce longitudinal magnetisation close to that obtained from a perfect 180° flip for $\xi \geqslant 0.75$. As ξ decreases below 0.75 the magnitude of the longitudinal magnetisation decreases for these frequency swept pulses, with the decrease largest for the HS and the second largest decrease for the SAR-matched SLAC-HS. The block pulse underflips for low ξ, flips accurately to 180° for $\xi = 1$ and overflips for high ξ. (For interpretation of the references to colour in this figure legend, the reader is referred to the web version of this article.)

early with ξ^{ref}, it has a clear maximum. Where SLAC is applied to the HS pulse the mean longitudinal magnetisation, C_z, is minimised around ξ^{ref} = 0.7, however, it stays relatively constant for choice of $\xi^{ref} > 0.7$ (Fig. 5d).

An overview of the simulated performance across pulse design parameters, pulse amplitude reference B_1 and pulse duration is illustrated using heatmaps (Fig. 6). Performance, denoted as C_{xy} (8), was evaluated as the mean value of the achieved transverse magnetisation across the simulated B_1 range. Fig. 6a–c show the performance for BIR-4, SAR-matched SLAC-BIR-4 and unscaled SLAC-BIR-4 respectively. The SAR-matched SLAC-BIR-4 outperforms the standard BIR-4 over a wide range of simulated pulse shapes (Fig. 6d) which highlights the performance difference. SAR-matched SLAC-BIR-4 pulses improve flip angle accuracy across a range of B_1 for longer pulse durations and lower reference B_1. The highest simulated increase in C was 13%. The chosen experimental parameters, T_p = 10 ms and ω_1^{ref} = 200 Hz, depict a standard adiabatic scenario and show a simulated increase in C of 2%. The simulation results for this case are displayed in Fig. 5 and demonstrate that this increase in C corresponds to an increase of

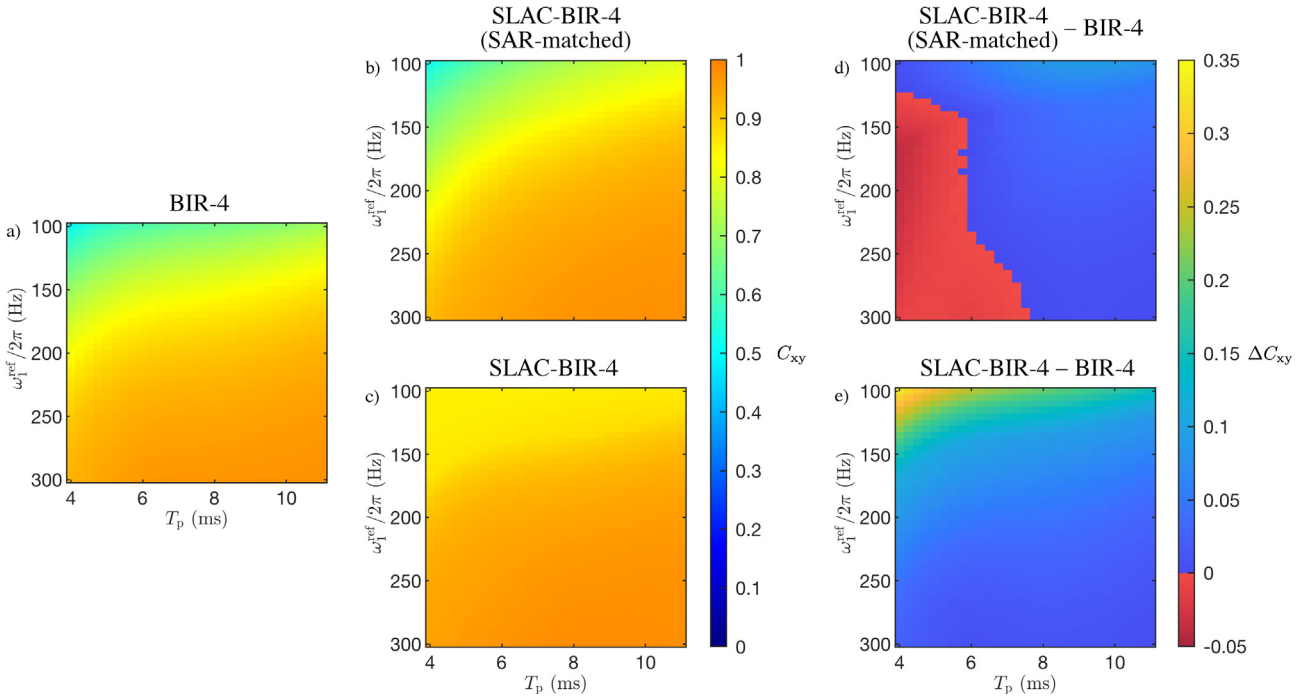

Fig. 6. Mean transverse magnetisation normalised by the desired transverse magnetisation, C_{xy}, following a 45° (a) BIR-4 pulse, (b) SAR-matched SLAC-BIR-4 pulse and (c) SLAC-BIR-4 pulse. The change in performance, ΔC_{xy}, relative to a BIR-4 pulse is shown for (d) SAR-matched SLAC-BIR-4 and (e) SLAC-BIR-4. A divergent colour scheme highlights the regions where performance is decreased (red) and improved (blue to yellow). Simulations were performed across pulse durations, T_p = (4–11 ms) and reference B_1 strength, $\omega_1^{ref}/2\pi$ = (100–300 Hz). Flip angle = 45°. The SAR-matched SLAC-BIR-4 pulse shows an improvement over the BIR-4 pulse across a large range of parameters. The SLAC-BIR-4 pulse produces greater performance than the BIR-4 pulse for all simulated pulse shape parameters. (For interpretation of the references to colour in this figure legend, the reader is referred to the web version of this article.)

7% in magnitude of transverse magnetisation for low B_1 field weighting factor, ξ. The unscaled SLAC-BIR-4 pulse shows clear improvements for all simulated pulse shape parameters (Fig. 6e).

SLAC targets B_1-insensitivity and only has a marginal effect on off-resonance performance (Fig. 7). In simulations, the region where magnetisation is within 5% of the desired magnetisation is a slightly different shape, however, the overall ranges of this level of performance are comparable for both adiabatic pulses and their SLAC equivalents. It should be noted that, close to resonance, SLAC-BIR-4 considerably reduces the oscillation of transverse magnetisation at largeB_1 field weighting factor, ξ.

A central transversal slice of the 3D volumes acquired with block, BIR-4 and SAR-matched SLAC-BIR-4 excitations are displayed in Fig. 8a–c, respectively. The block pulse results in very high image intensity within the central phantom region and very low image intensity in the bands above right and below left of the central region. In the BIR-4 and SLAC-BIR-4 images the image intensities in these regions are closer to the mean image intensity. This is consistent with the simulation of these pulses (Fig. 5a). The measured B_1 map (Fig. 8d) highlights that these hyper- and hypointense regions correspond to areas of high and low B_1 field strength, respectively. The differences between the images acquired with the SAR-matched SLAC-BIR-4 and standard BIR-4 pulse are analysed by examining the voxelwise ratio of the image intensities (Fig. 8e). It reveals an increase of around 4% in image intensity in the central region and an increase of around 10% in the darker regions adjacent to the central region.

A transversal single-slice volume acquired with using block, HS and SAR-matched SLAC-HS inversion pulse preparations are displayed in Fig. 9a–c, respectively. The block pulse results in very low image intensity within the central region and bottom edge of the phantom and, similarly, very low image intensity in the bands above right and below left of the central region. In the HS and SLAC-HS images the image intensities in these regions are much higher intensity. This is consistent with the simulation of these pulses (Fig. 5b). The measured B_1 map (Fig. 9d) highlights that these regions correspond to areas of high and low B_1 field strength, respectively. The differences between the images acquired with the SAR-matched SLAC-HS and standard HS pulse are analysed by examining the voxelwise ratio of the image intensities (Fig. 8e). It reveals an increase of around 4% in image intensity in the darker regions adjacent to the central region.

5. Discussion

SLAC is a new framework for improving the performance of adiabatic pulses. This method involves applying a correcting field to an adiabatic pulse in order to minimise the deviation which arises from restrictions on the rate at which the effective field is swept. The performance improvement was analysed in simulations and confirmed in experiment. SLAC pulses were found to outperform the BIR-4 and HS pulses upon which they were based and when rescaled to be equal in terms of SAR, SLAC pulses still maintained greater B_1 insensitivity than both BIR-4 and HS pulses while maintaining equivalent off-resonance performance.

Superadiabatic analysis [25,27] is able to reveal the angles between effective fields in higher adiabatic frames. When the adiabatic effective field, $B_{\mathrm{eff}}^{\mathrm{Ad}}$, and the magnetisation are initially collinear the trajectory of magnetisation is bounded by a cone of angle equal to the angle between the effective field in a given frame and the effective field in the previous frame. While the true trajectory of magnetisation is complicated by the rate of rotation in each adiabatic frame and by the angle between $B_{\mathrm{eff}}^{\mathrm{Ad}}$ and the magnetisation at the start of the pulse, links between cone angles and pulse performance can still be drawn. In the case of a truncated adiabatic pulse such as the HS pulse, the adiabatic effective field, $B_{\mathrm{eff}}^{\mathrm{Ad}}$, is slightly offset from the magnetisation at the beginning of the pulse and the upper bound of flip angle error is the sum of the field offset angle and the cone angle.

SLAC is targeted at reducing the cone angle in the first adiabatic frame. In the case that $\xi = \xi^{\mathrm{ref}}$, magnetisation is locked to the effective field perfectly in the FM frame. In other words, the cone is collapsed and the effective field is stationary in the first adiabatic frame. Subsequently, the effective field is stationary in all higher adiabatic frames. For the case that $\xi \neq \xi^{\mathrm{ref}}$ SLAC reduces the cone angle extremely effectively in the region where rate of change of the effective field is closest to linearly proportional to ξ. This is when $B_{\mathrm{eff}}^{\mathrm{Ad}}$ is close to the north pole of the Bloch sphere and in a

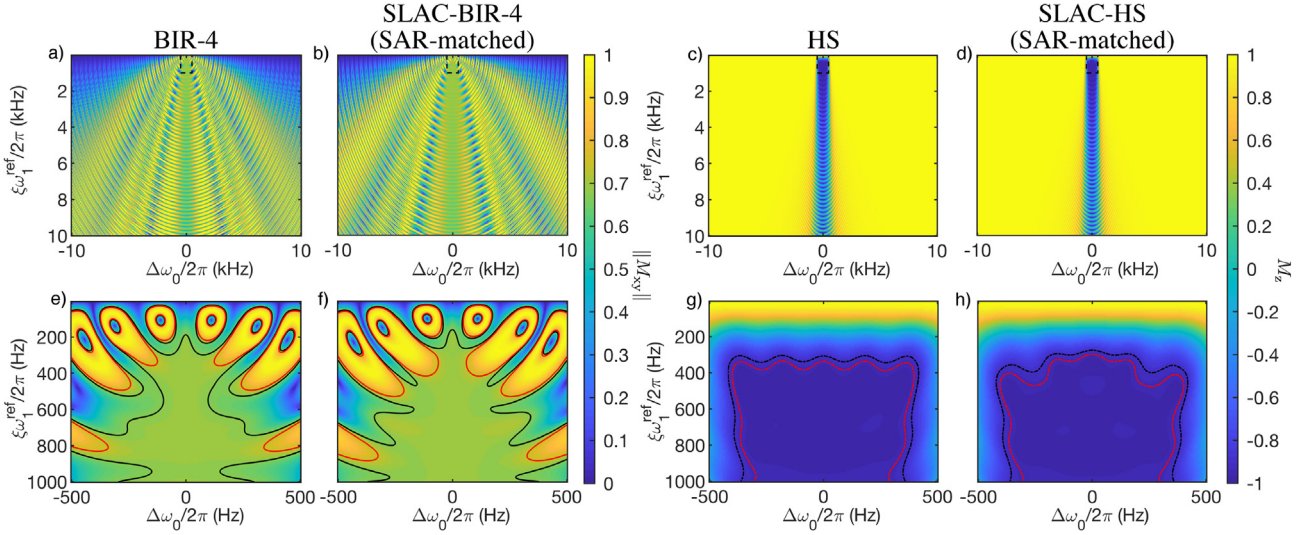

Fig. 7. The effect of resonance offset on magnitude of transverse magnetisation following a 45° (a) BIR-4 pulse and (b) SAR-matched SLAC-BIR-4 pulse. The effect of resonance offset on longitudinal magnetisation following a (c) HS pulse and (d) SAR-matched SLAC-HS pulse. Results corresponding to a reduced RF amplitude and resonance offset range corresponding to the dashed boxes in (a–d) are shown in (e–h) respectively. In (e–f) contour lines mark ±5% of the desired transverse magnetisation: solid black contour line = 0.95 sin(45°), solid red contour line = 1.05 sin(45°). In (g–h) contour lines mark 95% and 97.5% inversion: dashed black contour line = −0.9, dashed red contour line = −0.95. (For interpretation of the references to colour in this figure legend, the reader is referred to the web version of this article.)

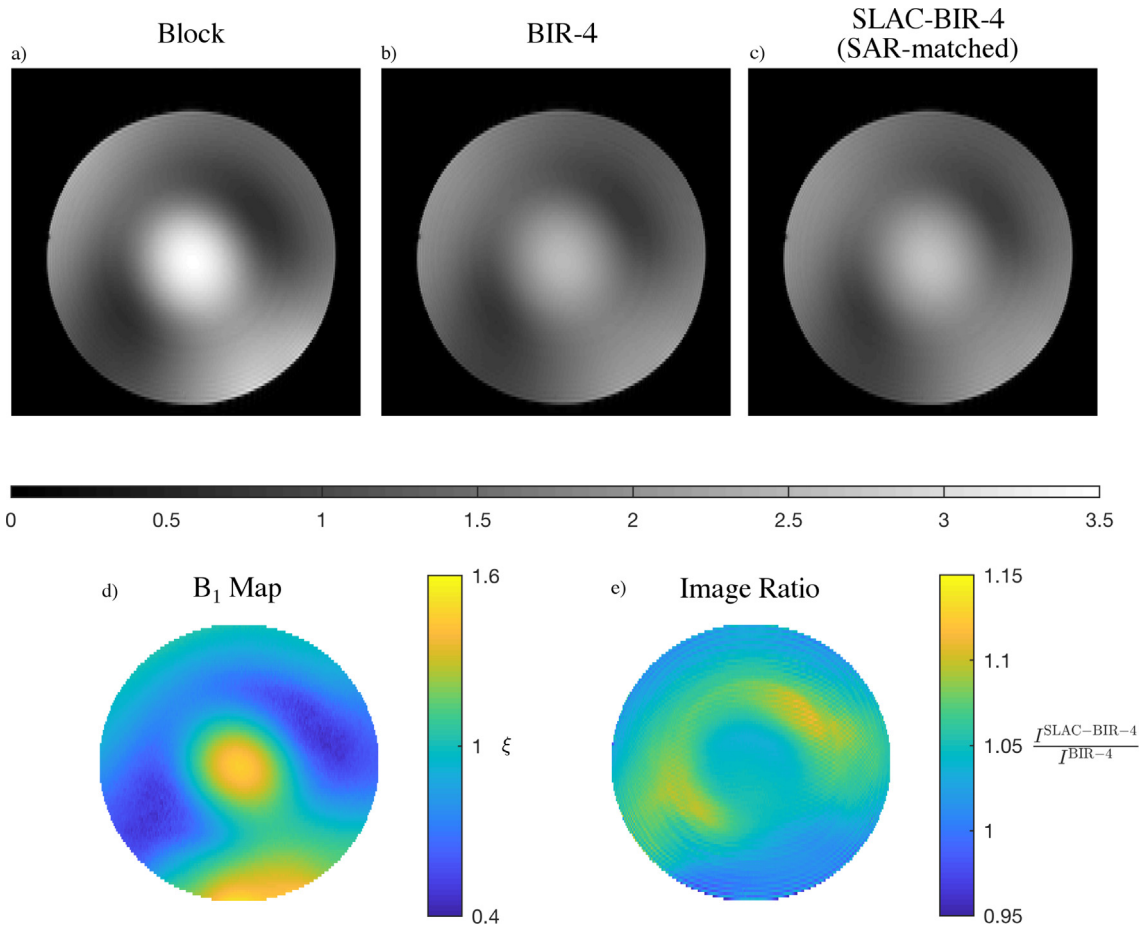

Fig. 8. Image acquired with (a) block pulse excitation, (b) BIR-4 pulse excitation, (c) SAR-matched SLAC-BIR-4 pulse excitation. (d) B_1 map of phantom produced from two single slice GRE images with excitation angles 45° and 90° using a double angle method. (e) Ratio image produced by voxelwise division of volume acquired with SAR-matched SLAC-BIR-4 pulse by volume acquired with BIR-4 pulse.

BIR-4 pulse this effect is seen at $T_p/4$ and $3T_p/4$ (Fig. 4). However, when B_{eff}^{Ad} is close to the equator of the Bloch sphere and the rate of change of the effective field is nonlinearly proportional to ξ, the B_1 field weighting factor range over which the correcting field is effective is reduced. This nonlinearity results in larger effective field angle derivatives which cause larger cone angles in higher adiabatic frames in the regions where ξ is vastly different from ξ^{ref}. To summarise what this means for pulse performance, the main presented advantage of SLAC is a decrease in the RF amplitude threshold at which the magnetisation is faithfully locked to the effective field (Fig. 5).

The importance of appropriately choosing ξ^{ref} should not be understated. While it has been shown that greater adiabaticity as a result of applying SLAC can cause an increase in performance, the choice of ξ^{ref} is critical for obtaining good adiabaticity across the ξ range of interest. As in Fig. 3, if ξ^{ref} is chosen too ambitiously a correction targeted far below the threshold for adiabaticity in the BIR-4 pulse results in compromised performance in a large section of the ξ range of interest. If ξ^{ref} is selected well above the adiabatic threshold, performance difference can be trivial. However, between these two extremes a value of ξ^{ref} can be chosen where the correcting field yields an improvement in the ξ range of interest while performance is maintained above this threshold. The values for ξ^{ref} used in simulation of SLAC-BIR-4 pulse performance across pulse duration, T_p and ω_1^{ref} were selected using a heuristic algorithm to produce values that gave a performance improvement. Further simulation of the effect of ξ^{ref} choice demonstrated the nonlinearity of performance as a function of ξ^{ref} choice for different pulse shapes (Fig. 3d). Optimisation of the choice of ξ^{ref} could give further gains in performance. In this first exposition of SLAC it is noted that experimental data has been acquired only for volume excitation and inversion and that both unscaled and SAR-matched SLAC envelopes have higher maximum amplitude than for the corresponding adiabatic pulse.

While here we have applied SLAC to a tanh/tan BIR-4 pulse and a HS pulse (Fig. 2), the concept is broadly applicable to all adiabatic pulses. Note that optimisation of adiabatic pulses and SLAC are not necessarily competing concepts; SLAC may be applied to envelopes that have already undergone an optimisation procedure. The SLAC approach is fundamentally different to numerically optimised modulation [23], while both methods focus on B_1 insensitivity through the lens of the adiabatic condition. The NOM approach modulates the time course through the envelope in order to slow changes in the effective field, as this is the source of departure from adiabaticity. NOM is applied with consideration to different field weighting factors and requires numerical integration in order to generate pulse envelopes. While NOM makes use of temporal modulation of amplitude and phase functions to minimise the $\frac{d\alpha}{dt}$ vector as it appears in the first adiabatic frame, SLAC makes use of an addition to the B_1 field to directly counteract it.

Other recent approaches to advance adiabatic pulses include pulses composed of shorter pulses either as a means of deriving an adiabatic pulse [28] or to make the pulse slice-selective by shaping the subpulses and applying a gradient, as the Slice-selective Tunable-flip Adiabatic Low peak-power Excitation

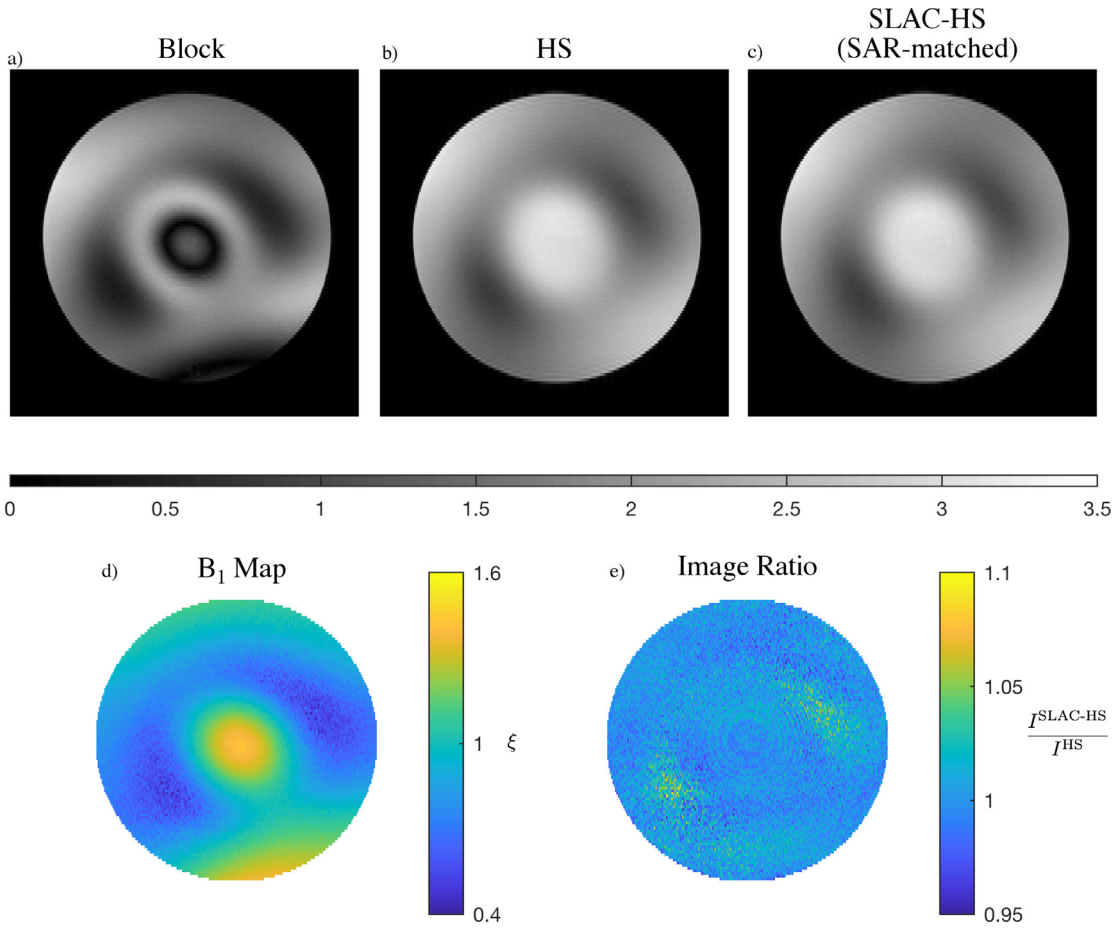

Fig. 9. Image acquired with (a) block pulse inversion, (b) HS pulse inversion, (c) SAR-matched SLAC-HS pulse inversion followed by sinc pulse excitation. (d) B_1 map of phantom produced from two single slice GRE images with excitation angles 45° and 90° using a double angle method. (e) Ratio image produced by voxelwise division of slice acquired with SAR-matched SLAC-HS pulse by slice acquired with HS pulse.

(STABLE) technique does [29]. These approaches can also be applied in combination with one another to yield further improvements in excitation [16]. Similarly, Moore et al. created B_1 insensitive composite pulses which could then be made slice-selective by shaping the subpulses and applying gradients [7,30]. It is anticipated that applying a technique such as STABLE to a SLAC pulse will enable slice-selection.

SLAC is applied with the aim of cancelling out an effective field component in the first adiabatic frame. It is able to be designed this way as the effective field that it is counteracting is always in the same plane as the B_1 field. However, there is the possibility that it could be beneficial to apply correcting fields in higher adiabatic frames. This would mean these fields would be composed of both a B_1 and a ΔB_0 component. Accounting for the nonlinear behaviour across a ξ range is a considerable challenge. Yet if this can be overcome, application of a ΔB_0 component that improves performance would result in improvements with no increased SAR cost and with no additional peak amplitude constraints. Although matching SAR, SLAC optimisation leads to higher peak RF amplitude which limits its application in situations where adiabatic pulses are applied at the maximum RF amplitude allowed by a given coil and amplifier. Further analysis of SLAC pulses that include the requirement of amplitude-matched ω_1 would be warranted in order to extend the utility of SLAC pulses. For example, a maximum amplitude constraint could also be addressed using amplitude modulation of B_1^{SL}. Further, while the presented approach is an optimisation for a single ξ value, future extensions could be based on optimisation of the adiabatic condition across a ξ range of interest.

6. Conclusion

A method for developing B_1 insensitive pulses based on an extension of adiabatic pulses has been demonstrated in theory, simulation and experiment. This method uses an additional field applied in concert with an arbitrary adiabatic pulse in order to lower the B_1 field amplitude threshold at which the desired magnetisation trajectory is maintained. When applied with a carefully chosen B_1 field amplitude weighting parameter, ξ^{ref}, this was shown to produce an increase in image intensity on the order of 10% in regions with low B_1 field weighting factor when compared with a BIR-4 pulse and an increase in image intensity of 4% in regions with low B_1 field weighting factor when compared with a HS pulse used as a preparation pulse. This method extends the possibilities of analytically derived B_1 insensitive pulse improvements and shows that these are applicable to practical 7T imaging sequences.

Declaration of Competing Interest

None.

Acknowledgment

We acknowledge the facilities, and the scientific and technical assistance of the Australian National Imaging Facility at the Melbourne Brain Centre Imaging Unit.

Appendix A

A.1. SLAC-BIR-4 pulse envelope equations

The equations required for implementation of the SLAC-BIR-4 pulse used in experiment and simulations are below. Eqs. (A.1), (A.2) and (A.3) come directly from previously described BIR-4 pulse envelopes [21]. Eq. (A.9) describes the amplitude of the additional component, derived from Eqs. (A.1) and (A.2) and the reference B_1 field weighting factor, ξ^{ref}, to which performance is tuned.

A.2. BIR-4 pulse equations

$$\omega_1^{\mathrm{Ad}}(t) = \omega_1^{\max}\tanh\left(\frac{\zeta(f(t))}{T_\mathrm{p}}\right) \tag{A.1}$$

$$\Delta\omega^{\mathrm{Ad}}(t) = \Delta\omega^{\max}\frac{\tan\left(\kappa(g(t)/T_\mathrm{p})\right)}{\tan(\kappa)} \tag{A.2}$$

$$\phi^{\mathrm{Ad}}(t) = \int_0^t \Delta\omega^{\mathrm{Ad}}(t')dt' + u(t-T_\mathrm{p}/4)\phi_1 + u(t-3T_\mathrm{p}/4)\phi_2 \tag{A.3}$$

$$f(t) = \begin{cases} T_\mathrm{p}/4 - t, & 0 \leqslant t \leqslant T_\mathrm{p}/4 \\ t - T_\mathrm{p}/4, & T_\mathrm{p}/4 < t \leqslant T_\mathrm{p}/2 \\ 3T_\mathrm{p}/4 - t, & T_\mathrm{p}/2 < t \leqslant 3T_\mathrm{p}/4 \\ t - 3T_\mathrm{p}/4, & 3T_\mathrm{p}/4 < t \leqslant T_\mathrm{p} \end{cases} \tag{A.4}$$

$$g(t) = \begin{cases} t & 0 \leqslant t \leqslant T_\mathrm{p}/4 \\ T_\mathrm{p}/2 - t, & T_\mathrm{p}/4 < t \leqslant T_\mathrm{p}/2 \\ t - T_\mathrm{p}/2, & T_\mathrm{p}/2 < t \leqslant 3T_\mathrm{p}/4 \\ T_\mathrm{p} - t, & 3T_\mathrm{p}/4 < t \leqslant T_\mathrm{p} \end{cases} \tag{A.5}$$

$$\phi_1 = \pi + \theta/2 \tag{A.6}$$

$$\phi_2 = \pi - \theta/2 \tag{A.7}$$

$$u(t) = \begin{cases} 0, & t < 0 \\ 1, & t \geqslant 0 \end{cases} \tag{A.8}$$

where θ is the flip angle.

A.3. Correcting component equations

Eqs. (A.9)–(A.11) are derived by substituting Eqs. (A.1) and (A.2) into Eqs. (2) and (5).

$$\omega_1^{\mathrm{SL}}(t) = \frac{N(t)}{D(t)}, \text{where} \tag{A.9}$$

$$N(t) = \frac{\omega_1^{\max}\zeta\tan(\kappa)\left(\tanh\left(\frac{\zeta(f(t))}{T_\mathrm{p}}\right)^2 - 1\right)}{\Delta\omega^{\max}T_\mathrm{p}\tan\left(\frac{\kappa g(t)}{T_\mathrm{p}}\right)} - \frac{\kappa\omega_1^{\max}\tanh\left(\frac{\zeta(f(t))}{T_\mathrm{p}}\right)\tan(\kappa)\left(\tan\left(\frac{\kappa g(t)}{T_\mathrm{p}}\right)^2 + 1\right)}{\Delta\omega^{\max}T_\mathrm{p}\tan\left(\frac{\kappa g(t)}{T_\mathrm{p}}\right)^2}, \tag{A.10}$$

$$D(t) = \left(\frac{\xi^{\mathrm{ref}}\omega_1^{\max}\tanh\left(\frac{\zeta(f(t))}{T_\mathrm{p}}\right)\tan(\kappa)}{\Delta\omega^{\max}\tan\left(\frac{\kappa g(t)}{T_\mathrm{p}}\right))}\right)^2 + 1, \tag{A.11}$$

Eqs. (A.1), (A.3) and (A.9) can then be substituted into Eq. (4) to yield the SLAC-BIR-4 pulse.

A.4. SLAC-HS pulse envelope equations

The equations required for implementation of the SLAC-HS pulse used in experiment and simulations are below. Eqs. (A.12), (A.13) and (A.14) come directly from previously described HS pulse envelopes [8]. Eq. (A.15) describes the amplitude of the additional component, derived from Eqs. (A.1) and (A.2) and the reference B_1 field weighting factor, ξ^{ref}, to which performance is tuned.

A.5. HS pulse equations

$$\omega_1^{\mathrm{Ad}}(t) = \omega_1^{\max}\mathrm{sech}\left(\beta(2t/T_\mathrm{p} - 1)\right) \tag{A.12}$$

$$\Delta\omega^{\mathrm{Ad}}(t) = \mu\beta\tanh\left(\beta(2t/T_\mathrm{p} - 1)\right) \tag{A.13}$$

$$\phi^{\mathrm{Ad}}(t) = \int_0^t \Delta\omega^{\mathrm{Ad}}(t')dt' \tag{A.14}$$

A.6. Correcting component equations

Eqs. (A.15), (A.16), (A.17) are derived by substituting Eqs. (A.12) and (A.13) into Eqs. (2) and (5).

$$\omega_1^{\mathrm{SL}}(t) = \frac{N(t)}{D(t)}, \text{where} \tag{A.15}$$

$$N(t) = \frac{2}{\mu T_\mathrm{p}}\omega_1^{\max}\mathrm{sech}\left(\beta\frac{2t}{T_\mathrm{p}}\right)\left(1 - \mathrm{cosech}^2\left(\beta\frac{2t}{T_\mathrm{p}}\right)\right), \tag{A.16}$$

$$D(t) = \left(\frac{\xi^{\mathrm{ref}}\omega_1^{\max}\mathrm{sech}\left(\beta\frac{2t}{T_\mathrm{p}}\right)}{\mu\beta\tanh\left(\beta\frac{2t}{T_\mathrm{p}}\right)}\right)^2 + 1, \tag{A.17}$$

Eqs. (A.12), (A.14) and (A.15) can then be substituted into Eq. (4) to yield the SLAC-HS pulse.

A.7. MATLAB code

MATLAB scripts for generation of pulse magnitude and phase for SLAC-BIR-4 and SLAC-HS pulses can be found at https://github.com/edwardmgreen/SLAC.

References

[1] Q.X. Yang, J. Wang, X. Zhang, C.M. Collins, M.B. Smith, H. Liu, X.-H. Zhu, J.T. Vaughan, K. Uğurbil, W. Chen, Analysis of wave behavior in lossy dielectric samples at high field, Magn. Reson. Med. 47 (5) (2002) 982–989.

[2] R. de Graaf, Y. Luo, M. Garwood, K. Nicolay, B_1-insensitive, single-shot localization and water suppression, J. Magn. Reson., Ser. B 113 (1) (1996) 35–45.

[3] J. Wang, M. Qiu, Q.X. Yang, M.B. Smith, R.T. Constable, Measurement and correction of transmitter and receiver induced nonuniformities in vivo, Magn. Reson. Med. 53 (2) (2005) 408–417.

[4] J.J. van Schie, C. Lavini, L.J. van Vliet, F.M. Vos, Feasibility of a fast method for B_1-inhomogeneity correction for FSPGR sequences, Magn. Reson. Med. 33 (3) (2015) 312–318.

[5] G. Adriany, P.-F. Van de Moortele, F. Wiesinger, S. Moeller, J.P. Strupp, P. Andersen, C. Snyder, X. Zhang, W. Chen, K.P. Pruessmann, P. Boesiger, T. Vaughan, K. Uğurbil, Transmit and receive transmission line arrays for 7 Tesla parallel imaging, Magn. Reson. Med. 53 (2) (2005) 434–445.

[6] Y. Zhu, Parallel excitation with an array of transmit coils, Magn. Reson. Med. 51 (4) (2004) 775–784.

[7] J. Moore, M. Jankiewicz, H. Zeng, A.W. Anderson, J.C. Gore, Composite RF pulses for B_1^+-insensitive volume excitation at 7 Tesla, J. Magn. Reson. 205 (1) (2010) 50–62.

[8] M. Garwood, L. DelaBarre, The return of the frequency sweep: designing adiabatic pulses for contemporary NMR, J. Magn. Reson. 153 (2) (2001) 155–177.

[9] N. Boulant, D. Le Bihan, A. Amadon, Strongly modulating pulses for counteracting RF inhomogeneity at high fields, Magn. Reson. Med. 60 (3) (2008) 701–708.

[10] M. Garwood, K. Uğurbil, RF pulse methods for use with surface coils: Frequency-modulated pulses and parallel transmission pulse methods for use with surface coils: frequency-modulated pulses and parallel transmission, J. Magn. Reson. 291 (2018) 84–93.

[11] R.S. Staewen, A.J. Johnson, B.D. Ross, T. Parrish, H. Merkle, M. Garwood, 3-D FLASH imaging using a single surface coil and a new adiabatic pulse, BIR-4, Invest. Radiol. 25 (5) (1990) 559–567.

[12] M.S. Silver, R.I. Joseph, D.I. Hoult, Highly selective $\pi/2$ and πpulse generation, J. Magn. Reson. 59 (2) (1984) 347–351.

[13] S. Conolly, D. Nishimura, A. Macovski, A selective adiabatic spin-echo pulse, J. Magn. Reson. 83 (2) (1989) 324–334.
[14] A.J. Johnson, M. Garwood, K. Uğurbil, Slice selection with gradient-modulated adiabatic excitation despite the presence of large B_1 inhomogeneities, J. Magn. Reson. 81 (3) (1989) 653–660.
[15] R.A. de Graaf, K. Nicolay, M. Garwood, Single-shot, b_1-insensitive slice selection with a gradient-modulated adiabatic pulse, BISS-8, Magn. Reson. Med. 35 (5) (1996) 652–657.
[16] P. Balchandani, G. Glover, J. Pauly, D. Spielman, Improved slice-selective adiabatic excitation, Magn. Reson. Med. 71 (1) (2014) 75–82.
[17] S. Conolly, J. Pauly, D. Nishimura, A. Macovski, Two-dimensional selective adiabatic pulses, Magn. Reson. Med. 24 (2) (1992) 302–313.
[18] M.A. Cloos, N. Boulant, M. Luong, G. Ferrand, E. Giacomini, D. Le Bihan, A. Amadon, kT-points: short three-dimensional tailored RF pulses for flip-angle homogenization over an extended volume, Magn. Reson. Med. 67 (1) (2012) 72–80.
[19] A. Jang, X. Wu, E.J. Auerbach, M. Garwood, Designing 3D selective adiabatic radiofrequency pulses with single and parallel transmission, Magn. Reson. Med. 79 (2) (2018) 701–710.
[20] M. Mullen, N. Kobayashi, M. Garwood, Two-dimensional frequency-swept pulse with resilience to both B_1 and B_0 inhomogeneity, J. Magn. Reson. 299 (2019) 93–100.
[21] M. Garwood, Y. Ke, Symmetric pulses to induce arbitrary flip angles with compensation for RF inhomogeneity and resonance offsets, J. Magn. Reson. 94 (3) (1991) 511–525.
[22] M.R. Bendall, D.T. Pegg, Uniform sample excitation with surface coils for in vivo spectroscopy by adiabatic rapid half passage, J. Magn. Reson. 67 (1986) 376–381.
[23] K. Uğurbil, M. Garwood, A.R. Rath, Optimization of modulation functions to improve insensitivity of adiabatic pulses to variations in B_1 magnitude, J. Magn. Reson. 80 (3) (1988) 448–469.
[24] A. Tannús, M. Garwood, Improved performance of frequency-swept pulses using offset-independent adiabaticity, J. Magn. Reson., Ser. A 120 (1) (1996) 133–137.
[25] M. Deschamps, G. Kervern, D. Massiot, G. Pintacuda, L. Emsley, P.J. Grandinetti, Superadiabaticity in magnetic resonance, J. Chem. Phys. 129 (20) (2008) 204110.
[26] E. Insko, L. Bolinger, Mapping of the radiofrequency field, J. Magn. Reson., Ser. A 103 (1) (1993) 82–85.
[27] D. Rosenfeld, Y. Zur, Is the sech/tanh adiabatic pulse really adiabatic?, J Magn. Reson. 132 (1) (1998) 102–108.
[28] P. Balchandani, J. Pauly, D. Spielman, Designing adiabatic radio frequency pulses using the Shinnar-Le Roux algorithm, Magn. Reson. Med. 64 (3) (2010) 843–851.
[29] P. Balchandani, J. Pauly, D. Spielman, Slice-selective tunable-flip adiabatic low peak-power excitation pulse, Magn. Reson. Med. 59 (5) (2008) 1072–1078.
[30] J. Moore, M. Jankiewicz, A.W. Anderson, J.C. Gore, Slice-selective excitation with B_1^+-insensitive composite pulses, J. Magn. Reson. 214 (2012) 200–211.